Treatment of Systematic Errors in the Processing of Wide-Angle Sonar Sensor Data for Robotic Navigation

MARTIN BECKERMAN, MEMBER, IEEE, AND E. M. OBLOW

Abstract—**A methodology has been developed for the treatment of systematic errors, which arise in the processing of sparse sensor data. A detailed application of this methodology to the construction, from wide-angle sonar sensor data, of navigation maps for use in autonomous robotic navigation is presented. In the methodology, a four-valued labeling scheme and a simple logic for label combination are introduced. The four labels, conflict, occupied, empty, and unknown, are used to mark the cells of the navigation maps. The logic allows for the rapid updating of these maps as new information is acquired. The systematic errors are treated by relabeling conflicting pixel assignments. Most of the new labels are obtained from analyses of the characteristic patterns of conflict that arise during the information processing. The remaining labels are determined by imposing an elementary consistent-labeling condition.**

I. INTRODUCTION

IN this work, we describe a methodology for the treatment of systematic errors that arise in the processing of sparse sensor data. We introduce the various components of the methodology while presenting a detailed application to the processing of sonar range information for use in navigation by the HERMIES-IIB mobile robot of the Center for Engineering Systems Advanced Research (CESAR) at the Oak Ridge National Laboratory (ORNL). The function of the methodology in this application is to enable the robot to build a reliable internal spatial representation of the world, that is, a navigation map, for which there is otherwise no prior information.

A. Experimental Test Bed

HERMIES-IIB is one of a series of research robots designed for autonomous navigation in unknown and possibly hazardous terrain. The robot is described in depth by Burks *et al.* [2]. In brief, it is equipped with vision sensors, an on-board 16-node NCUBE hypercube parallel computer, and an on-board AT host computer. The HERMIES-IIB robot is also equipped with 24 ultrasonic transducers for range sensing. These are grouped into six-phased arrays of four units each. The units contained Polaroid industrial-grade transducers and produced a 50-kHz burst that was 1 ms in duration.

The transducers function as both transmitter and receiver of ultrasound. In the sonarlike sensing process, the time of flight for the returned signal is measured. Given the velocity of sound, the range to the scattering source is then determined. Intensity information is not recorded; instead, the earliest return signal is processed. Thus, the distance to the nearest object lying either wholly or partially within the beam is determined, and the region lying inside the beam at shorter distances than that of the scattering source is established as being unoccupied.

In the experiments, range data were taken in 15° steps over the full 360° field. The beam width of the sonar units is broad. In the phased configuration, the effective beam width is approximately 18°. The selection of a 15° angular step size is based on the observation that because of the broad beam width, data collected in smaller steps are highly redundant. The step size chosen allows for a reasonable amount of overlap between adjacent data points while providing an efficient probe of the test space.

B. Systematic Errors

The sonar range sensors, as used, give rise to a variety of systematic errors (see, for example, [10]). By systematic errors, we mean those errors that result from incorrect and inconsistent interpretations of the data during processing. The ultrasound systematic processing errors depend upon the beam width or resolution, the radiated power and sensing threshold of the sensors, and the environmental geometry and surface properties of the objects being sensed. The beam width at typical sensing distances is comparable to the dimensions of many of the objects in the robot's environment. Commonly encountered systematic errors include 1) distortions in size and orientation of the object surfaces and 2) specular reflections from hard, smooth surfaces. In the latter case, desirable signals can be produced by both scattering and specular reflections, but multiple reflections lead to artifacts.

By definition of our test bed, we do not have detailed information about the environment and the properties of the object surfaces. Therefore, we cannot model the physics of the sensing process sufficiently well to remove the systematic errors prior to processing. Instead, we observe that there are several possible interpretations of the data from a given isolated scan. When combining data from different sensing positions or angles, erroneous initial interpretations will give rise to recognizable patterns of conflict. Whenever this happens, we can use physical arguments to guide the replacement of erroneous interpretations with those that are consistent with the new information. Not all systematic errors can be so

Manuscript received March 18, 1988. This work was supported by the Office of Basic Energy Sciences and the Office of Technology Support Programs, U.S. Department of Energy, under Contract DE-AC05-84OR21400 with Martin Marietta Energy Systems, Inc.

The authors are with the Engineering Physics and Mathematics Division, Oak Ridge National Laboratory, Oak Ridge, TN 37831.

IEEE Log Number 8933169.

1042-296X/90/0400-0137$01.00

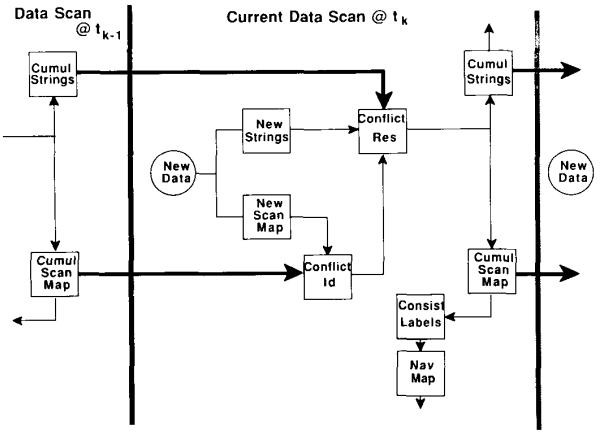

Fig. 1. Time-sliced flowchart showing conflict identification, conflict resolution (pattern analysis), and consistent-labeling algorithm in relation to appropriate data structures.

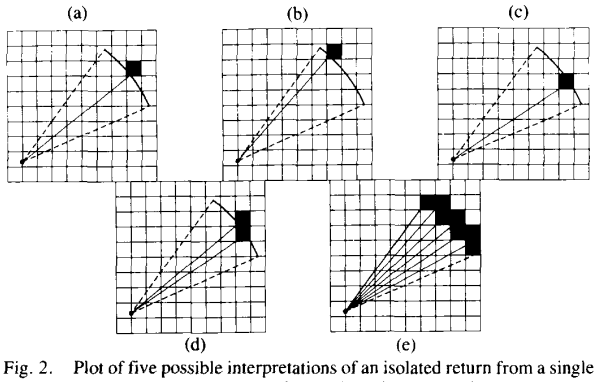

Fig. 2. Plot of five possible interpretations of an isolated return from a single scan. Arcs are not drawn to scale in this and the following figures.

treated, and such a methodology is best suited to the case where the data are sparse, the patterns of conflict are simple, and the corrections are physically unambiguous.

As indicated in Fig. 1, there are distinct conflict identification and resolution stages in our methodology. In the identification stage, four labels are introduced to delineate occupied, empty, unknown, and conflict cells of the robot's cumulative map. The conflict label is used to denote cells that have been identified to be occupied in one measurement and empty in another measurement. In the resolution stage, two physical statements are made that are valid for objects in our test bed: 1) a real ultrasound beam cannot pass through a real object, and 2) there are no point objects. These statements take the form of a pattern analysis and a consistent-labeling algorithm, respectively.

C. Objectives

The extent to which we are successful in identifying and resolving the resulting conflicts and uncertainties is determined by examining the two-dimensional navigation maps constructed from the sonar data. These maps should have accurately and clearly delineated open spaces and obstacles. Another objective is to ensure that the methodology allows for the extraction of progressively higher level features, which may be integrated with the commensurate vision data. The importance of computation maps as key building blocks in the infrastructure of the low- and intermediate-level information processing in the nervous system has been documented in studies by Knudsen *et al.* [18], Takahashi and Konishi [26], and Sullivan and Konishi [25]. For example, computational maps of interaural delay, interaural intensity difference, and space all contribute to the spatial analysis of sound. Although our maps are not computational maps in the nervous system, they do serve an analogous physiological function. These maps are, of course, software constructs designed for a machine and its sensors. At the present level of sensor integration, the maps are the robot's internal representation of the world. It is therefore important to examine the roles played by higher level inferencing in the constructing of such maps from sparse and incomplete data.

II. Information Processing

A. Possible Interpretations of an Isolated Return

The principal systematic errors considered herein are those related to the broad beam width of the sensors. Fig. 2 shows schematic representations of some of the possible interpretations of the scan return from a single scan angle. The arcs drawn in the figure denote the angular width of the beams, which was taken as 18°. These arcs are shown superimposed upon a rectangular grid defining the bins (pixels) into which the information will be stored. The situation depicted in Fig. 2(a) corresponds to interpreting the scattering source as lying along the centerline (beam axis) at the distance given by the range finder. A single pixel not lying along the beam axis is viewed as being occupied by the scattering source in Fig. 2(b) and (c); a pair of pixels are occupied in Fig. 2(d), and all pixels intercepted by the arc are interpreted as the scattering source in Fig. 2(e).

In processing our sparse data, we initially adopt interpretation (e), in which all possible occupied pixels are taken as such, to be the one best representing the scattering source. The implementation for a single isolated return consists of labeling those pixels lying along the arc as occupied and scoring all pixels located inside the region bounded by the endpoint rays and the arc as empty. Underlying the selection of interpretation (e) is a world view, specifically, that the robot's universe consists of extended objects (relative to the geometric size represented by a pixel). This world view may be contrasted to, say, one for a world containing only well-separated point objects. In such a point-object world, possibilities of types (a) to (c) would be more appropriate.

B. Multiple Returns and Patterns of Conflict

In Fig. 3, we represent data from two scan returns covering a common region of interest. Fig. 3(a) and (b) depicts the returns from a pair of adjacent scan angles from a single observation point. In Fig. 3(c) and (d), the robot is scanning overlapping regions of space from two different viewing points. In each of the four examples, there is some conflict in the results of applying the interpretation in Fig. 2(e) to the scan

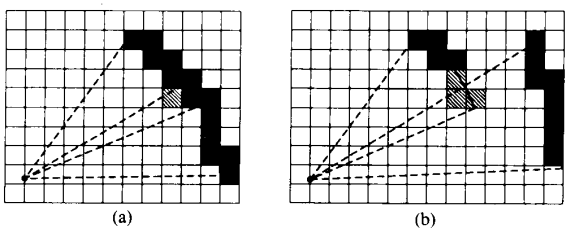

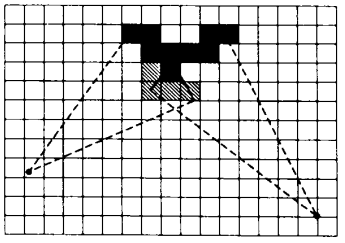

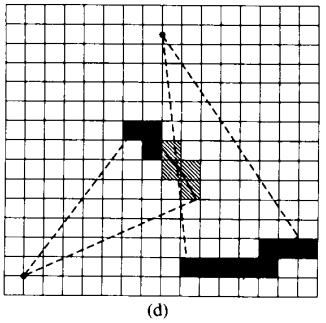

Fig. 3. Plot of representative pixel patterns. Heavily shaded cells denote occupied pixels. Cross hatched cells have conflict label assignments.

pairs. The methodology at this point consists of identifying the conflict generated among the pixel labels and then resolving this conflict to achieve a consistent interpretation of the data.

C. Labels and Their Logic

To process the information from two (or more) scans, we perform pixel-by-pixel multiplication using the rule of combination

$$L_{ij}^{A} \cap L_{ij}^{B} = L_{ij}^{C}$$

where L_{ij} denotes the label for the ijth pixel, and superscripts A and B identify the pair of measurements leading to the new result C. The conflict label differs from the occupied and empty labels in that two returns are needed for its assignment. In set terminology, we may use the conflict element to represent the simultaneous intersection of occupied and empty elements. If we define the unknown element as the union of occupied and empty, we can use the intersection operator as our rule of label combination, as indicated in the above expression. Fig. 4 gives the results so derived, with $C = O \cap E$ and $U = O \cup E$.

An essential feature of this labeling scheme is its quaternary character. This labeling representation allows for the pattern

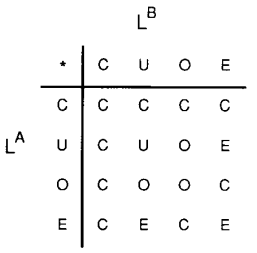

Fig. 4. Logic for label combination.

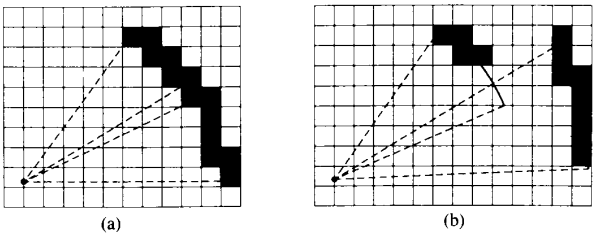

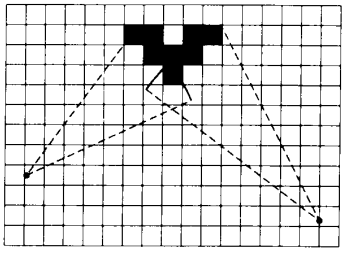

Fig. 5. Corrected plot of representative pixel patterns showing pixel patterns (a) to (c) of Fig. 3 after pattern analysis.

analyses discussed in the next section. It may be noted that two of the labels U and C are, in a sense, place holders for the physical labels O and E.

The pixel-by-pixel multiplication was coded using the label representation

$$C=0, \qquad U=1, \qquad O=2, \qquad E=3.$$

The 16 possible binary products were then evaluated by executing the statement

$$\text{if } L^A = L^B, \text{ then } L^C = L^A; \text{ else } L^C = L^A \times L^B \bmod 6.$$

The first (if) part of this statement (written here in an obvious, nontechnical notation) handles the four diagonal entries in the table, whereas the 12 off-diagonal elements were handled by the second (else) part, and $L = C$, U, O, or E. Returning to Fig. 3, we find that conflict pixel labels are assigned in the overlap region, where the cells are marked empty in one measurement and occupied in the other.

D. Pattern Analysis

Fig. 5 presents the analyzed and corrected interpretations of the patterns initially given in Fig. 3. We see in these diagrams that all uncertain pixel assignments have been resolved with the replacement of conflict with empty labels. The physical

reason for this replacement is that a real sonar beam cannot pass through a real object in its path.

For instance, the systematic error flagged by the conflict label in Fig. 5(a) arises as a result of a slight disparity between the (curved) locus of possible occupied cells and the actual surface of the object. Specifically, the arcs tend to identify pixels that are progressively too close to the beam origin as the surface normal increasingly departs from orthogonality to the beam direction. The correct interpretation is to take the longer of the two possible returns at each viewing angle as being correct since those returns should lie closer to the actual surface.

In Fig. 5(b), we have an example where the two arcs have rather different ranges. If the ranges are similar, we have the situation in Fig. 5(a), and we assume that there is a single extended scattering source and apply the correction just discussed. If the ranges are not similar, then we may assume that there is more than one scattering source. If the cells in question were occupied, then the longer of the two returns would not have been received. Thus, the only consistent interpretation is that the pixels with conflicting labels are empty. The effect of this correction upon the nearby object is similar to that of an erosion (as opposed to a dilation) operation in vision information processing.

Before discussing the pattern type in Fig. 5(c), we observe in Fig. 1 that there are data structures called strings. By strings, we mean sequences of returns of similar range from adjacent scan angles bounded at both ends by depth discontinuities. Strings are the interesting features in the ultrasound scene, marking the possible locations of object surfaces. They represent the extension of the sequences of occupied pixels illustrated in Figs. 3 and 5 to instances where there are two or more continuous ranges. As such, strings comprise the first order of feature extraction above the pixel level and are in this sense comparable to edges in visual image processing. To facilitate the pattern analyses, navigation, and integration with vision data, complete information on each string is stored.

The situation shown in Fig. 5(c) is one in which two strings intersect one another at some angle. This type of pattern is produced by distortion errors. It arises because the initial processing using the maximal set (Fig. 2(e)) tends to exaggerate the spatial extent of surfaces. We correct for this as additional data are collected by relabeling as empty those pixels that are flagged by the ensuing conflicts. This can be done for any string-crossing angle. The particular case shown as Fig. 5(c) is for a string-crossing angle of approximately 90° and thus resembles a corner. Situations of near-zero string-crossing angle also occur. In those cases (not illustrated), the viewing angles are nearly the same, although the ranges differ. The apparent size of any surface will be greater when seen at the longer distance, and the two sets of data are made consistent by relabeling as empty the flagged cells at the left and right ends.

No pattern has been presented in Fig. 5 for case (d), in which one string interdicts the empty zone of a second, nonintersecting string. This pattern of conflict is simple, but the corrections are not unambiguous. The conflict can occur whenever the size distortions are large for either string; it can also occur when there are specular reflections. The mean ranges of the strings are stored in the string data structures in order to provide some, albeit limited, means for resolving the conflict. This pattern of conflict is discussed further in Section III-C.

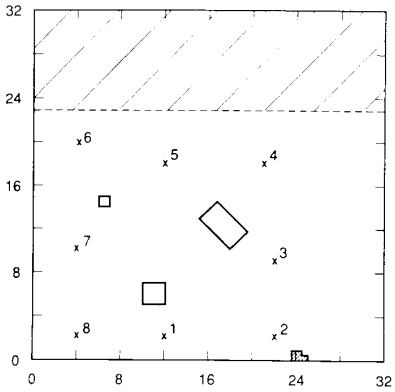

Fig. 6. Schematic diagram of experimental configuration used in CESAR laboratory. Numbers show eight scan locations of the HERMIES-IIB robot; the open squares and rectangle represent obstacles. Not shown is the wall on the left, which is located at −1 ft. Also missing are a workstation plus some partitions placed along the right side of the lab, as well as some low-level clutter in the upper right-hand corner.

III. Maps and Pattern Analyses

A. Laboratory Environment and Robot Navigation

Plotted in Fig. 6 is a portion of the CESAR laboratory, which was set up with three objects of different sizes and orientations. There are a 2-by-2-ft box, a larger 2-by-4-ft box, and a small 1-by-1-ft box. All three boxes are tall enough to intercept the sonar viewing plane. Shown in the plot is the location of the back wall of the laboratory. This wall tends to specularly reflect the sonar signals, as does the wall on the left-hand side of the room (which is off scale). Finally, there are a support pillar and an adjacent pair of narrow vertical pipes in the lower right-hand corner of the room. Displayed along with these five "objects" are eight locations along the path taken by the HERMIES-IIB robot. At each of these locations, a 360° scan was taken in 24 15° steps (except the first position, where small angular steps were used).

In navigating about our test environment, cumulative dead-reckoning errors can occur. This class of errors has been discussed by Chatila and Laumond [5] and Drumheller [6]. In their studies, a number of solutions were investigated, and those introduced previously in the literature were cited. Spatial uncertainties due to dead-reckoning errors have also been examined by Smith *et al.* [23], [24]. In the present work, we avoided these errors by explicit placement of the robot at the various test locations. We did this for two reasons. First, we wanted to focus our attention on the systematic errors discussed in the earlier sections. Second, we wanted to maintain a clear separation between model-building (mapping) and path-planning issues.

B. Instantaneous Scan Maps and Strings

In building the new, or instantaneous, scan maps, all pixels were initially considered to be unknown. To identify the pixels

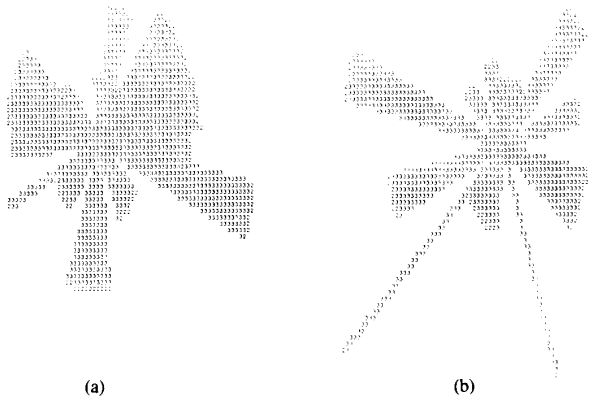

(a) (b)

Fig. 7. Instantaneous scan maps: (a) Map built from data taken at position 5; (b) map constructed from data acquired at position 4. Maps are 64 × 64 pixels.

located along the beam arcs, synthetic beams of identical range were generated (by the software) at intermediate angles. A stepsize of 2° was chosen as being adequate to cover the region of interest. The unoccupied region was then swept out by finding all pixels intercepted by the rays drawn at each intermediate angle from the occupied domain to the robot origin. All pixels for which there was no information from the robot's sensors due to either occlusions or the sensor's finite horizon remain marked unknown.

The results of processing the sparse information from a single 360° scan are presented in Fig. 7. Conflicts represented by the patterns shown in Figs. 3(a) and (b) and 5(a) and (b) were resolved when the synthetic beams were generated. At this level of processing, conflicts of type (c) have not been identified. Instead, they will be treated during the construction of the cumulative scan map to be described shortly. The dimensions of all maps were chosen as 64 × 64 pixels, and each pixel denotes a 6-in-square region of space. The pixels of the instantaneous (single) scan map carry one of three labels: unknown (1), occupied (2), or empty (3).

We observe in Fig. 7 that the measurement serves to partition the space into a number of distinct regions. The most prominent of these are the empty zones that fan out from the robot origin and terminate at strings. The important strings in, for example, Fig. 7(a) are located at the ends of the three zones fanning out in a downward direction from the robot origin to the surfaces of the three boxes. To exhibit these strings in a clear visual manner, we have suppressed the processing of all but a few long returns for which no echo was received.

It should be observed that in our analysis, extended objects are perceived as having smoothly joined surfaces. There are, for example, no intersecting wedge-shaped objects, and deeply convoluted surfaces will not be seen as such. This aspect is part of our world view, which was introduced in Section II, and is consistent with the physical limitations of the sensor.

C. Cumulative Scan Maps

Fig. 8 displays a sequence of eight cumulative scan maps corresponding to the eight scanning positions shown in Fig. 6. All rays have been included in the scoring. For purposes of visual display, unknown areas were left blank, and occupied regions were marked with x's. We observe in this progression of maps that regions that are initially occluded or out of range of the sensor are gradually identified, and the outlines of the boxes are built as their various surfaces are illuminated. By the eighth scan, all three boxes are delineated.

To construct the cumulative scan map, we performed a map-by-map multiplication, that is, the label of the ijth pixel in the instantaneous (scan) map was multiplied by the label of the ijth pixel in the previously updated cumulative map, and the results were stored as the new label of the ijth pixel in the new cumulative map. The label multiplication was done for all pixels using the logic presented in Fig. 4. The pixels of the cumulative scan map, therefore, take on the values of conflict (0), unknown (1), occupied (2), or empty (3).

At this point, the data were examined for conflict patterns of the type shown in Fig. 3(c). The pattern analysis was done using an auxiliary 64 × 64 array and the string data structures shown in Fig. 1. Each element of the array, or map, contains the addresses of the most recently acquired data structure entry for that spatial location. Each data structure entry contains the length of the string, that is, the number of pixel elements, the mean range, the (x, y) string coordinates, and the address of the entry corresponding to the next most recently acquired string passing through that spatial location. This information was used to check rapidly for string-crossing places where a pair of strings cross through one another. In those instances where this occurred, any conflict labels lying along either of the strings were replaced with empty labels, as indicated in Fig. 5(c).

In the final stage of preparation of the cumulative scan map, we make a limited attempt to treat conflict patterns of type 3(d). Our objective was to minimize the destruction of legitimate occupied labels by the incorrect marking of empty pixels during the processing of specular reflections. These most often give rise to long returns, and their incorrect interpretation can give rise to the pattern shown as Fig. 3(d). If conflicting assignments were encountered between elements of a string seen at short range and empty zones swept out by distant returns, the conflict was resolved by selection of the occupied label.

IV. Consistent Labeling and Navigation Maps

A. Consistent Labeling

The final information-processing stage consists of converting residual conflict labels to occupied or empty labels. We carry out this operation by imposing a consistent-labeling requirement, namely, that the label must be consistent with those of its neighbors. Underlying this operation is the physical argument that there are no point objects in the robot's environment.

The 3 × 3 mask shown in Fig. 9 is used in the consistent-labeling algorithm. As illustrated in this figure, the values of the labels of the four nearest-neighbor pixels are added together. If their sum (threshold value) is above a fixed value, the pixel in question is considered to be empty; otherwise, there is a cluster or poorly defined string, and the pixel is marked occupied.

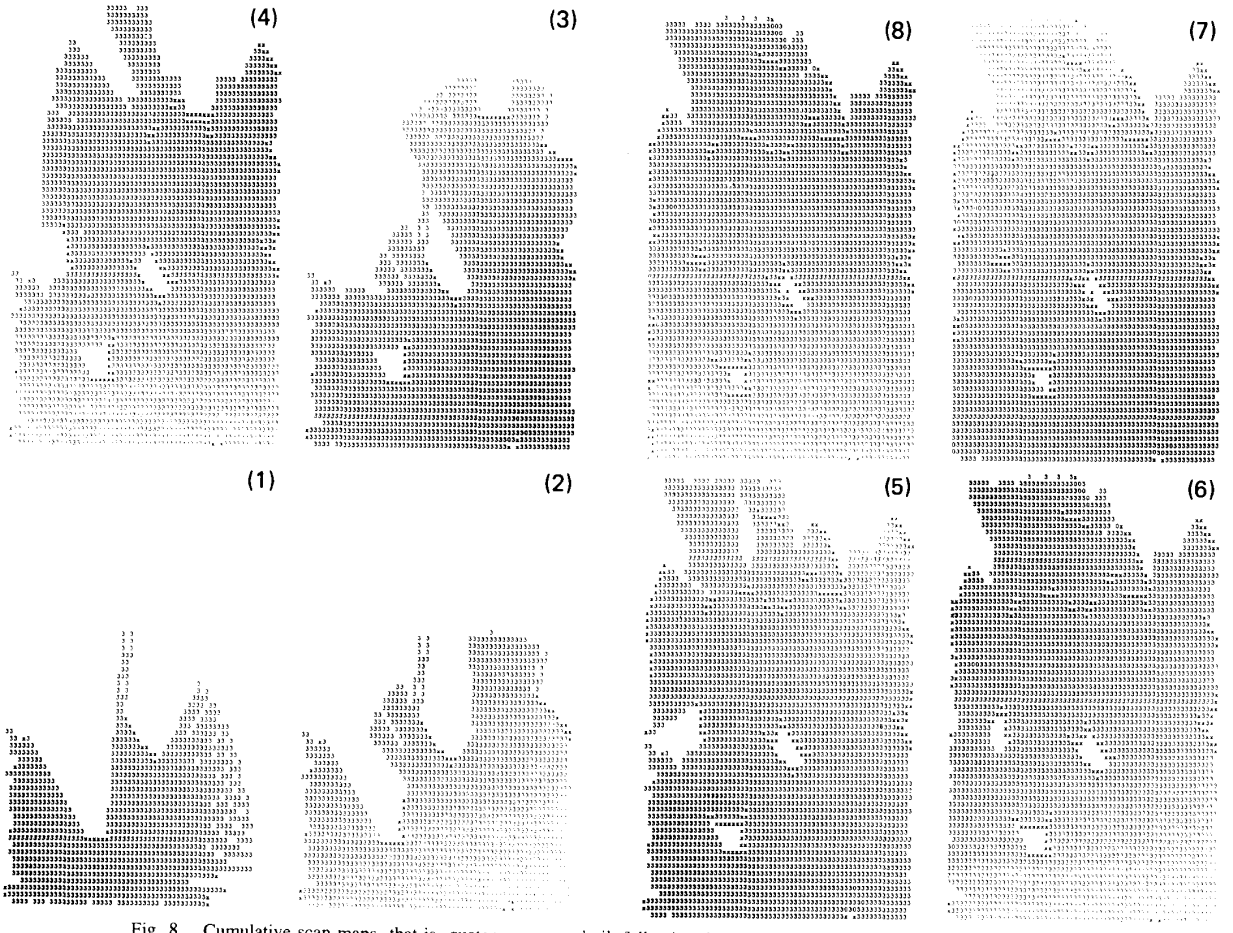

Fig. 8. Cumulative scan maps, that is, quaternary maps built following data collection at the eight scan sites in Fig. 6.

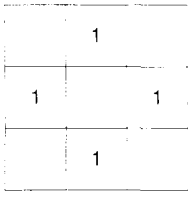

Fig. 9. Mask used for consistent labeling.

The utility of the consistent-labeling operation is twofold. First, it effects the removal of isolated conflict labels. These labels are produced by processing errors involving strings of unit length. This aspect of the consistent-labeling operation is one of filtering to produce a clean map for navigation. Second, the operation converts clusters of conflict labels that may occur in the vicinity of object surfaces to occupied labels.

This second use is one of preserving sparse information on occupied regions. The second feature becomes important whenever objects, such as the small 1-by-1-ft box, and the pillar located in the lower right-hand corner of the laboratory are poorly defined by the data. The operation helps further to preserve strings against destruction by the labeling of empty zones corresponding to specular reflections.

The criterion for treating a conflict cluster as a valid object surface is given by the value for the threshold used in the algorithm. The threshold value, in turn, depends upon the angular step size for the generation of the synthetic beams. For example, for the 2° step size used in the construction of the previous maps, a value of 6 or 7 is optimal, whereas for a 3° step size, a value of 9 is more appropriate. (A 3° stepsize, although adequate for short- and intermediate-distance returns, may miss some of the 6-by-6-in pixels at large distances. For such cases, that is, when the sensing horizons are greater than about 10 ft, an angular step size of 2° will lead to a complete sweep of the cells lying within the beam.)

Finally, it may be noted that the consistent-labeling algorithm can be applied to the removal of embedded unknown labels produced by an inadequate angular step size. In Fig. 1, we observe that the residual uncertainties are removed by the consistent-labeling operations only during the reduction to a binary navigation map, that is, consistent label changes are not retained, but instead, the algorithms are reapplied each time sensor data are achieved. This is done to maintain consistency of interpretation among the various data sets.

B. Navigation Maps

Two types of navigation maps—tertiary and binary—can be built once the consistent-labeling operation is completed. Cells

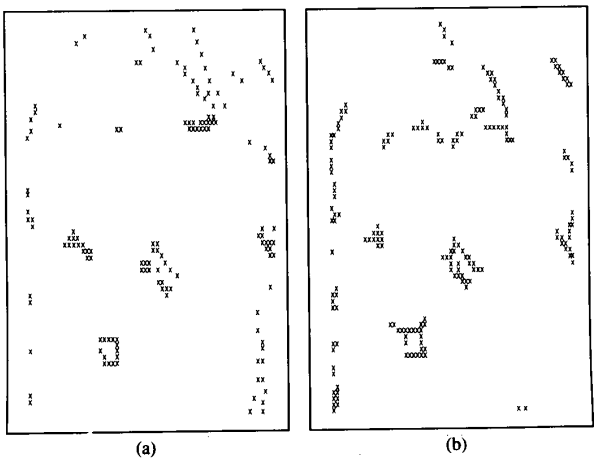

Fig. 10. Cumulative navigation maps at the end of data collection: (a) Horizon = 25.5 ft, angstep = 3°, conlab threshold = 9, and pattern-(d) maximum range = 6 ft.; (b) horizon = 18 ft, angstep = 2°, conlab threshold = 7, pattern-(d) maximum range = 12 ft.

of the tertiary map carry one of three labels: occupied, empty, or unknown, whereas cells of the binary map possess one of two labels: occupied or empty. The choice of map is dictated by its use in the robotic system. Retention of the unknown label is useful when executing searches since it denotes regions not yet probed by the sensors. If the only objective is navigation, then unknown and occupied labels are, in effect, identical, indicating regions of space that are not available for passage by the robot.

Fig. 10 shows a pair of binary navigation maps produced at the end of the final 360° scan. These binary maps differ from the corresponding tertiary maps only in the labeling of a few pixels at the far top and bottom. In constructing the figure, we tried to highlight the occupied cells. To do this, we changed the displayed occupied pixel label to an $\times$; all others are shown as blanks.

The two maps shown in Fig. 10 were produced from the same data. The differences between them are due to changes made in the maximum range of the sensors (Horizon), angular step size used to generate the synthetic beams, consistent labeling threshold (Section IV-A), and the maximum range before a return is treated as "distant" (Section III-C) used in the processing. We observe that the three boxes are clearly delineated in each of the maps, and the spaces between and around them are free from "debris" as well. Upon comparing the two maps, we see that the 2-by-2-ft box is more clearly outlined in Fig. 10(a). However, the small 1-by-1-ft box, back wall, and support pillar, for which the data are sparse, are better defined in the map in Fig. 10(b).

In both maps in Fig. 10, the small 1-by-1-ft box appears somewhat larger than its actual size. The systematic size exaggeration has been reduced considerably by the pattern analysis (c) and by the consistent-labeling operation. The extent of the reduction can be seen by comparing the representation of the box in the instantaneous scan maps (Fig. 7) to that appearing in the cumulative navigation maps (Fig. 10). The dependence of the apparent size of objects upon the distance of observation can also be observed by comparing the lengths of the strings denoting the presence of the 1-by-1-ft box in Fig. 7. In fact, using the information provided by overlapping sensor measurements, we can localize objects to dimensions smaller than the beam width.

In Fig. 10(a), we see that the back wall of the laboratory does not appear to be well defined. This wall extends from the left side to the right side of the room, as indicated in Fig. 6. In place of a clearly defined wall, we find a few occupied pixels at the correct position, plus several strings situated beyond the wall. These strings, clearly visible in Fig. 7, were produced by our processing of false specular reflections from the hard, smooth back wall. (In addition to the back wall, the left face of the 2-by-2-ft box tended to specularly reflect the sonar signals due to the poor viewing angles. As a result, it was not as well delineated as the other faces.)

The map presented in Fig. 10(b) corresponds to the instantaneous and cumulative scan maps displayed in Figs. 7 and 8. The back wall is better defined in Fig. 10(b) as a result of the use of a shorter sensor horizon and parameters that better enable the pattern analysis to preserve correctly processed strings. In this navigation map, most of the data on the wall present in the instantaneous (new) scan maps have been retained.

Turning to the literature, we note that the strings of pixels lying behind the back wall cannot be removed using the test of Drumheller [6] since we do not assume prior knowledge of the existence of walls. Additional sharpening of object surfaces can be accomplished by performing fits to straight-line segments and to polygons. The usefulness of these object-localization techniques has been demonstrated by Drumheller [6], Chatila and Laumond [5], Gaston and Lozano-Perez [12], Grimson and Lozano-Perez [13], and Grimson [14]. In incorporating these techniques, one should ensure that the higher level features so extracted remain consistent with the world view of the lower level data-processing stage. Finally, we note that effects of errors on the construction of two-dimensional visual maps have been investigated by Brooks [1].

There are a number of possible strategies for reducing

uncertainties in object location due to specular reflections. On a hardware level, we note that bats use a broad range of ultrasonic frequencies for echo location (see, for example, Fenton and Fullard [9]), and we might try to eliminate specular reflections by using an adaptive sensor. On a software level, lowering the sensor horizon to distances on the order of 8–15 ft, plus increasing the scan frequency, would serve to increase the reliability of the navigation maps in the presence of specularly reflecting surfaces. Specular reflections from smooth walls have been studied and modeled by Kuc and Siegel [19], [20], and the mathematical problem of finding surface normals has been investigated by Brown [3], [4]. The identification of specular reflections is being addressed further by us in an extension of the present methodology to multisensor fusion. Those results will be reported elsewhere.

V. Discussion of Some Alternative Approaches

Methodologies for the storage of information from sonar range sensors in the form of Cartesian maps have been presented by Elfes [7], [8], Moravec and Elfes [21], and Moravec [22] at Carnegie-Mellon University (CMU) and by Fryxell [11] at ORNL. The CMU methodology made use of probability distributions, and Fryxell used a voting procedure to represent initial information on occupied and empty regions of space. In both stochastic approaches, cumulative information, stored in separate "occupied" and "empty" maps, was used to generate a binary navigation map.

Stochastic methods are, of course, well established and suited for the treatment of random errors. The emphasis in the present work was on developing some means for treating systematic, not random, errors. We were motivated by the observation that it would be useful to have simple, nonstochastic methods for the identification and removal of systematic errors from the processing of sparse sensor data. A methodology of this type was presented herein for the processing of ultrasound data. In comparing the two classes of approaches as applied to ultrasound, we observe that the stochastic approaches were local in character, that is, the reduction of the various probabilities or votes to one or two labels was done for any given pixel using only information pertaining to that pixel. That type of methodology may be contrasted with our nonlocal approach, which made use of information about neighboring cells and maintained self-consistency between occupied and empty regions of space. In doing so, we employed labels termed unknown and conflict, whose meanings differed from that of appellation "uncertain," as used in the CMU work.

Systematic errors predominate over random errors in the processing of our ultrasound data. It is therefore to be expected that we can build more sharply delineated maps using our method than can be obtained in the alternative, stochastic approaches. This point was checked in detail by comparing our navigation maps with those constructed by the voting procedure. This was a meaningful comparison since the same laboratory environment was probed by identical sensors in both studies. Our finding is that even though five times as many data were collected in the voting experiments, the objects appearing in the maps generated in the present experiments were more clearly delineated. This proved to be the case even when we decreased our cell resolution to match that used by Fryxell.

VI. Summary and Concluding Remarks

To summarize, a methodology has been developed for the identification and removal of systematic errors as they arise in the processing of sparse and incomplete sensor data. We have introduced the components of the methodology as applied to the processing of range information acquired by the HERMIES-IIB mobile robot using its wide-angle ultrasound sensors. We have seen that the Cartesian maps, comprising the robot's internal representation of the world, contained clearly delineated occupied and empty regions of space.

Our approach made use of overlapping measurements and a multivalued labeling scheme and was explicitly nonlocal. The systematic errors manifested themselves as conflicts between initial interpretations of overlapping data and were flagged by a conflict label as new information was gathered. The quaternary character of our approach enabled us to do a spatial pattern analysis and impose simple consistent-labeling conditions to remove the conflicts once they were identified. These and the other processing operations we have described are well established in the field (see, for example, Haralick and Shapiro [15], [16] and Hummel and Zucker [17]) and have been used extensively for different purposes in information processing. In the present application, these operations, and the underlying physical arguments, have provided the means to do straightforward, compact, sufficient mapping calculations for data that are correctly position registered.

Finally, we have taken the first steps to extract progressively higher level features from the data. This aspect, and the compatibility of our information processing with that of vision, should provide a useful framework for multisensor (sonar + vision) integration.

Acknowledgment

The authors wish to acknowledge the many valuable discussions held throughout the course of this work with R. C. Mann, F. G. Pin, and C. R. Weisbin. The authors also wish to acknowledge the assistance provided by D. L. Barnett, E. Lyness, and M. Kedl in the HERMIES-IIB experiments. Finally, the authors wish to thank R. Fryxell for making available his ray-scoring routine, which was used with only minor changes in the present work.

References

[1] R. A. Brooks, "Visual maps for a mobile robot," in *Proc. IEEE Int. Conf. Robotics Automat.*, 1985, pp. 824–829.

[2] B. L. Burks, G. de Saussure, C. R. Weisbin, J. P. Jones, and W. R. Hamel, "Autonomous navigation, exploration, and recognition using the HERMIES-IIB robot," *IEEE Expert*, vol. 2, pp. 18–27, 1987.

[3] M. K. Brown, "Locating object surfaces with an ultrasonic range sensor," in *Proc. IEEE Int. Conf. Robotics Automat.*, 1985, pp. 110–115.

[4] M. K. Brown, "Feature extraction techniques for recognizing solid objects with an ultrasonic range sensor," *IEEE J. Robotics Automat.*, vol. RA-1, pp. 191–205, 1985.

[5] R. Chatila and J.-P. Laumond, "Position referencing and consistent world modelling for mobile robots," in *Proc. IEEE Int. Conf. Robotics Automat.*, 1985, pp. 138–145.

[6] M. Drumheller, "Mobile robot localization using sonar," *IEEE Trans. Patt. Anal., Mach. Intell.*, vol. PAMI-9, pp. 325–332, 1987.

[7] A. Elfes, "Multiple levels of representation and problem solving using maps from sonar data," in *Proc. DOE/CESAR Workshop Planning Sensing Autonomous Navigation* (C. R. Weisbin, Ed.) (Los Angeles, CA), 1985, pp. 17-34.
[8] A. Elfes, "A sonar-based mapping and navigation system," in *Proc. IEEE Int. Conf. Robotics Automat.*, 1986, pp. 1151-1156.
[9] M. B. Fenton and J. H. Fullard, "Moth hearing and the feeding strategies of bats," *Am. Sci.*, vol. 69, pp. 266-275, 1981.
[10] A. Flynn, "Redundant sensors for mobile robot navigation," M.S. thesis, Dept. Elec. Eng. Comput. Sci., M.I.T., Cambridge, MA, Sept. 1985.
[11] R. C. Fryxell, "Navigation planning using quadtrees," ORNL/TM-10481 (CESAR-87/20), 1987.
[12] P. G. Gaston and T. Lozano-Perez, "Tactile recognition and localization using object models: The case of polyhedra on a plane," *IEEE Trans. Patt. Anal., Mach. Intell.*, vol. PAMI-6, pp. 257-266, 1984.
[13] W. E. L. Grimson and T. Lozano-Perez, "Recognition and localization of overlapping parts from sparse data in two and three dimensions," in *Proc. IEEE Int. Conf. Robotics Automat.*, 1985, pp. 61-66.
[14] W. E. L. Grimson, "Sensing strategies for disambiguating among multiple objects in known poses," *IEEE J. Robotics Automat.*, vol. RA-2, pp. 196-213, 1986.
[15] R. M. Haralick and L. G. Shapiro, "The consistent labelling problem: Part I," *IEEE Trans. Patt. Anal., Mach. Intell.*, vol. PAMI-1, pp. 173-184, 1979.
[16] R. M. Haralick and L. G. Shapiro, "The consistent labelling problem: Part II," *IEEE Trans. Patt. Anal., Mach. Intell.*, vol. PAMI-2, pp. 193-203, 1980.
[17] R. A. Hummel and S. W. Zucker, "On the foundations of relaxation labelling processes," *IEEE Trans. Patt. Anal., Mach. Intell.*, vol. PAMI-5, pp. 267-287, 1983.
[18] E. I. Knudsen, S. du Lac, and S. D. Esterly, "Computational maps in the brain," *Ann. Rev. Neurosci.*, vol. 10, pp. 41-65, 1987.
[19] R. Kuc and M. W. Siegel, "Efficient representation of reflecting structures for a sonar navigation model," in *Proc. IEEE Int. Conf. Robotics Automat.*, 1987, pp. 1116-1123.
[20] R. Kuc and M. W. Siegel, "Physically based simulation model for acoustic sensor robot navigation," *IEEE Trans. Patt. Anal., Mach. Intell.*, vol. PAMI-9, pp. 766-778, 1987.
[21] H. P. Moravec and A. Elfes, "High resolution maps from wide angle sonar," in *Proc. IEEE Int. Conf. Robotics Automat.*, 1985, pp. 116-121.
[22] H. P. Moravec, "Certainty grids for mobile robots," in *Proc. JPL Workshop Telerobotics* (Pasadena, CA), Jan. 1987.
[23] R. C. Smith and P. Cheeseman, "On the representation and estimation of spatial uncertainty," *Int. J. Robotics Res.*, vol. 5, pp. 56-68, 1986.
[24] R. Smith, M. Self, and P. Cheeseman, "A stochastic map for uncertain spatial relationships," in *Proc. IEEE Int. Conf. Robotics Automat.*, 1987, p. 850.
[25] W. E. Sullivan and M. Konishi, "Neural maps of interaural phase difference in the owl's brainstem," *Proc. Nat. Acad. Sci.*, vol. 83, pp. 8400-8404, 1986.
[26] T. Takahashi and M. Konishi, "Selectivity for interaural time difference in the owl's midbrain," *J. Neurosci.*, vol. 6, pp. 3413-3422, 1986.

Martin Beckerman (M'89) received the B.S. and M.S. degrees in physics from the University of Florida, Gainesville, in 1964 and 1966, respectively, and the Ph.D. degree in physics from the University of Miami in 1970. He was awarded a NASA Predoctoral Fellowship for the 1967 to 1970 academic years.

He was an Institute Fellow in the Department of Nuclear Physics of the Weizmann Institute of Science from 1972 to 1974 and a Research Scientist and Principal Investigator in the Laboratory for Nuclear Science of the Massachusetts Institute of Technology from 1979 to 1984. During that time he discovered the anomalous subbarrier fusion of atomic nuclei. He served as Associate Professor of Physics at the University of Tennessee from 1984 to 1986. He was a consultant to the Kellogg Radiation Laboratory of the California Institute of Technology in 1983 and to the Physics Division of the Oak Ridge National Laboratory, Oak Ridge, TN, in 1984. During that time, he discovered the anomalous subbarrier fusion of Division at ORNL in 1987. He has authored over 80 publications in robotics and in experimental and theoretical nuclear physics. His research interests include adaptive sensing, sensor modeling, sensor fusion, and image model building.

E. M. Oblow was born in 1942. He received the B.Eng.S. degree from City College, New York, in 1965 and the M.S. and Ph.D. degrees from Columbia University, New York, in 1970. Major fields of study were applied mathematics, nuclear physics, and engineering.

Currently, he is a Senior Research Staff Member of the Engineering Physics and Mathematics Division at Oak Ridge National Laboratory, Oak Ridge, TN. His research interests include sensitivity and uncertainty theory, computer calculus, artificial intelligence, and parallel computing. He authored over 100 papers and reports and was responsible for the development of adjoint sensitivity theory and its implementation in computer calculus.